J Nanopart Res (2017) 19:101
DOI 10.1007/s11051-017-3805-y

RESEARCH PAPER

Effects of PEGylation on biomimetic synthesis of magnetoferritin nanoparticles

Caiyun Yang · Changqian Cao · Yao Cai · Huangtao Xu · Tongwei Zhang · Yongxin Pan

Received: 14 December 2016 / Accepted: 21 February 2017

Abstract Recent studies have demonstrated that ferrimagnetic magnetoferritin nanoparticles are a promising novel magnetic nanomaterial in biomedical applications, including biocatalysis, imaging, diagnostics, and tumor therapy. Here we investigated the PEGylation of human H-ferritin (HFn) proteins and the possible influence on biomimetic synthesis of magnetoferritin nanoparticles. The outer surface of HFn proteins was chemically modified with different PEG molecular weights (PEG10K and PEG20K) and different modification ratios (HFn subunit:PEG20K = 1:1, 1:2, 1:4). The PEGylated HFn proteins were used for biomimetic synthesis of ferrimagnetic magnetoferritin nanoparticles. We found that, compared with magnetoferritin using non-PEGylated HFn protein templates, the synthesized magnetoferritin using the PEGylated HFn protein templates possessed larger magnetite cores, higher magnetization and relaxivity values, and improved thermal stability. These results suggest that the PEGylation of H-ferritin may improve the biomineralization of magnetoferritin nanoparticles and enhance their biomedical applications.

Keywords Ferritin · PEGylation · Biomimetic synthesis · Magnetic nanoparticles · Biomedical applications

Introduction

Nanoparticles possess unique physical and chemical properties different from bulk material due to the quantum size effect (Burda et al. 2005), which continue to attract immense research interest and are increasely important for many technological applications. Nanoparticles like Au, ZnO, and Fe_3O_4 are used in a wide

C. Yang · C. Cao · Y. Cai · H. Xu · T. Zhang · Y. Pan
Key Laboratory of Earth and Planetary Physics, Institute of Geology and Geophysics, Chinese Academy of Sciences, Beijing, People's Republic of China

C. Yang
e-mail: ycy@mail.iggcas.ac.cn

C. Cao
e-mail: changqiancao@mail.iggcas.ac.cn

Y. Cai
e-mail: caiyao@mail.iggcas.ac.cn

H. Xu
e-mail: xuhuangtao@mail.iggcas.ac.cn

T. Zhang
e-mail: ztw@mail.iggcas.ac.cn

C. Yang · C. Cao · Y. Cai · H. Xu · T. Zhang · Y. Pan (✉)
France-China Bio-Mineralization and Nano-Structures Laboratory, Chinese Academy of Sciences, Beijing, People's Republic of China
e-mail: yxpan@mail.iggcas.ac.cn

C. Yang · H. Xu
University of Chinese Academy of Sciences, Beijing, People's Republic of China

Published online: 09 March 2017

range of fields, such as biomedicine (e.g., Dreaden et al. 2012), optoelectronic devices (e.g., Yu et al. 2016), imaging (e.g., Cao et al. 2014; Uchida et al. 2008), catalysis (e.g., Fan et al. 2012; Zhang et al. 2017), and diagnostics and tumor therapy (e.g., Fantechi et al. 2014; Uchida et al. 2006). In the past decade, magnetic nanoparticles have been intensively developed (e.g., Pankhurst et al. 2016; Laurent et al. 2010; Burtea et al. 2005; Fan et al. 2003; Kohler et al. 2006). Conventional synthesis of magnetic nanoparticles is through chemical or physical approaches, which are sometimes cumbersome and often require specialized surface coating in order to be nontoxic, biocompatible, and targetable (Ding et al. 2012; Gao et al. 2009; Tromsdorf et al. 2009). Ferritin, a widely existing iron-storage protein in many living organisms throughout animals, plants, and bacteria (Theil 1987), is a cage-like protein with an external diameter of 12 nm and an inner diameter of 8 nm (Harrison and Arosio 1996). The structure of mature mammalian ferritin consists of a 24-subunit protein (450–500 KD), which is composed of heavy-subunits (H; ~21 KD) and light-subunits (L; ~19 KD) (Harrison et al. 1967). Within the ferritin protein cavity, there is a very weak magnetic hydrous ferric oxyhydroxide (ferrihydrite) mineral core. Due to its intrinsic cage-like structure, there are great interests in synthesis of various strongly ferrimagnetic nanoparticles using ferritin proteins (Douglas et al. 1995; Kramer et al. 2004; Mann et al. 1993; Mann and Meldrum 1991; Yamashita et al. 2004; Cao et al. 2010). Meldrum and coworkers obtained demetalized horse spleen ferritin (apoferritin) by removing the ferrihydrite core and were the first to successfully synthesize a magnetic mineral (magnetite) within apoferritin, named as magnetoferritin (Meldrum et al. 1992). Recently, through advancements in genetic engineering, the recombinant human H-chain ferritin (HFn) was developed and used to synthesize monodispersed, non-interacting ferrimagnetic magnetoferritin nanoparticles (hereafter named as M-HFn). These magnetoferritins have stoichiometric magnetite cores with nearly spherical shape, extremely narrow size distribution, high crystallinity, and are superparamagnetic at ambient temperature (e.g., Uchida et al. 2006; Uchida et al. 2008; Cao et al. 2010; Walls et al. 2013; Melnikova et al. 2014; Cai et al. 2015; Zhang et al. 2017). Importantly, it has been well demonstrated that the M-HFn nanoparticles can be directly used to visualize diverse tumor tissues, due to their dual functionality of active tumor-targeting ability and inherited peroxidase-like activity (Fan et al. 2012; Cao et al. 2014; Zhang et al. 2017).

Polyethylene glycol (PEG) is an amphiphilic monodisperse polymer with high degree of segmental flexibility in aqueous solutions and extensively used in protein modification (Delgado et al. 1992; Veronese 2001; Roberts et al. 2002). The PEGylation modification of proteins has been found very useful in preventing aggregation, improving half-lives, and reducing toxicity (Kinstler et al. 1996; Uchio et al. 1999; Hinds and Kim 2002; Harris and Chess 2003; Lu et al. 2008; Wynn and Gumuscu 2016). With distinct interfaces, ferritin could be modified with PEG to reduce immunogenicity, increase half-life (Vannucci et al. 2012; Fantechi et al. 2014), improve water solubility, design a tumor-environment-responsive nanocarrier (Matsumura et al. 2011), and link HFt with antibody molecules (Falvo et al. 2013). On the other hand, it has been reported that PEGylation of ferritin is able to suppress bulk precipitation during biomimetic synthesis of cobalt-oxide core (Co_3O_4) (Tsukamoto et al. 2008). However, the effect of PEGylation on biomineralization of magnetoferritin is still poorly understood. Whether PEGylation influences the biological activity of ferritin and what effect PEGylation has on the biomineralization of the magnetite cores of magnetoferritin nanoparticles requires further investigations.

In the present study, we synthesized a series of PEGylated HFn with different molecular weights (PEG10K, PEG20K; HFn subunit:PEG = 1:4) and different molecular ratios (HFn subunit:PEG20K = 1:1, 1:2, 1:4). These PEGylated HFn cages were then used as biotemplates to synthesize magnetoferritin (M-HFn-PEG) nanoparticles. In order to assess the influence of PEGylation on magnetite biomineralization, the synthesized M-HFn-PEG nanoparticles were characterized through measuring the core size, magnetic properties, iron content, relaxivity, and thermal stability, and related mechanisms are discussed.

Materials and methods

Preparation of recombinant human H-chain ferritin (HFn) The *Escherichia coli* strain *Rosetta*, which carries recombinant plasmid pET11b-*HFn*, was cultured in Luria-Bertani medium at 37 °C. Ampicillin was introduced as selection markers. The isopropyl-β-D-thiogalactopyranoside (IPTG, 1 mM) was added after

3 h as an inductive agent to induce the expression of ferritin at 30 °C. After 10 h, cells were collected by centrifugation and then dispersed using phosphate buffer saline (PBS, pH 7.4). The entire thallus was sonicated on ice for 5 min, followed by centrifugation (10,000 g, 20 min, Eppendorf Centrifuge 5810 R). The supernatant from centrifugation was heat-treated at 75 °C for 15 min to remove the thermolabile protein. In order to eliminate impurity, the HFn was further purified through size exclusion chromatography (Sepharose 6B, GE Healthcare). The purified HFn were analyzed by sodium dodecyl sulfate polyacrylamide gel electrophoresis (SDS-PAGE). The protein concentration was measured using BCA protein assay kit (Pierce) with bovine serum albumin as standard.

PEGylation of HFn The HFn was modified with different PEG molecular weights (10 and 20 K, a molar ratio of 1:4; hereafter defined as HFn-PEG10K and HFn-PEG20K, respectively) and different PEG molecular ratio HFn subunit:PEG20K = 1:1, 1:2, 1:4 (hereafter named as HFn-PEG20K(1:1), HFn-PEG20K(1:2), HFn-PEG20K(1:4), respectively). The PEG derivatives (methoxy-PEG-N-hydroxysuccinimide, mPEG-NHS) were purchased from JenKem Technology, USA. In the PEGylation process, mPEG-NHS was firstly dissolved in 1 mL sodium phosphate buffer (0.01 M, pH 2). Then, purified ferritin was incubated with mPEG-NHS in sodium phosphate buffer (0.01 M, pH 8.5) at room temperature with stirring for 4 h to link PEG to HFn and form PEGylated HFn. To get rid of extra unlinked PEG from the products, the reaction mixture was further purified using size exclusion chromatography (Sepharose 6B, GE Healthcare). The synthesized PEGylated HFn was adjusted to 3 μg and examined by 13.5% SDS-PAGE. Afterwards, the gels were incubated in barium chloride/iodine solutions and Coomassie brilliant blue R250 staining solution. The gel was washed 2–3 times using ddH_2O and incubated in an aqueous solution of 5% barium chloride for 20–30 min. After washing 2–3 times, 0.1 M iodine solution was added for specifically staining the PEG. The gel was then re-stained with Coomassie brilliant blue R250 staining solution to visualize the protein band.

Synthesis of M-HFn-PEG nanoparticles The ferrimagnetic M-HFn-PEG nanoparticles were synthesized according to our previous method with some modifications (Cao et al. 2010). An average of 5000 iron atoms were loaded into HFn and HFn-PEG, respectively; the synthesized M-HFn and M-HFn-PEG nanoparticles are named as M-HFn_{5000} and M-HFn-PEG_{5000}, respectively. The synthesized nanoparticles were centrifuged for 20 min at 10,000 g and then passed through the size exclusion chromatography (Sepharose 6B, GE Healthcare) for further purification. The bicinchoninic acid (BCA) protein assay reagent was used for protein quantitation.

Iron uptake analysis of HFn-PEG The iron uptake rate experiments were carried out at room temperature. Specifically, 10 mM ammonium ferrous sulfate was freshly prepared using 4.95 mg/mL thiourea solution. Thiourea was used to prevent auto-oxidation of Fe^{2+}. A solution of 0.1 M HEPES (pH 7.0) was prepared for reaction buffer. After rapid mixing of 25 μL 1 mg/mL HFn-PEG in 1965 μL HEPES and 10 μL Fe^{2+} solution, the mixture was monitored in a UV/Visible spectrophotometer for 1200 s at wavelength of 310 nm.

Inductively coupled plasma mass spectrometry (ICP-MS) analysis The inductively coupled plasma mass spectrometry (ICP-MS) (Agilent, 7500A) was used to determine the average iron content of M-HFn-PEG nanoparticles. A 50 μL solution of these samples was transferred to a heat-resistant container. All samples were nitrified three times in a clean room using high-purity hydrogen nitrate at 160 °C and diluted with 1 M hydrogen nitrate to 1 mL. The average number of iron atoms per protein was calculated from ICP-MS data according to the standard curve of iron.

Transmission electron microscopy and circular dichroism spectra analysis The core size and crystallinity of synthesized nanoparticles were analyzed by transmission electron microscopy (TEM; JEOL JEM-2100). The nanoparticles were desalted in a PD-10 desalting column (GE Healthcare) and deposited onto ultrathin amorphous-carbon films. TEM analysis was performed at an accelerating voltage of 200 KV.

Circular dichroism (CD) spectroscopy is used to examine the secondary structures of HFn-PEG cage, including α-helical, β-sheet, and random coil regions, after mineralization. The sample was diluted to a concentration of 0.15 mg/mL and tested using a cup with diameter of 0.5 mm on a Chirascan™-Plus CD spectrometer (Applied Photophysics, Leatherhead, UK) at 200–260 nm (bandwidth: 1 nm).

Magnetic property analysis The M-HFn-PEG nanoparticles were freeze-dried using an Alpha 1-2 LD plus freeze drier. The samples were place inside a non-magnetic capsule and measured on a Quantum Design MPMS SQUID magnetometer (Model XP-XL5, with magnetic moment sensitivity of 5.0×10^{-10} Am^2). Low-field thermal demagnetization curves were measured between 5 and 200 K in a steady field of 1.5 mT. After the zero-field cooling from 200 to 5 K, zero-field cooling (ZFC) curve was measured. The field-cooled (FC) curve was then measured after being field-cooled from 200 to 5 K in a field of 1.5 mT. The blocking temperature (T_b) was determined from the measurements of ZFC-FC cycling. The isothermal remanent magnetization (IRM) acquisition and DC demagnetization curves were measured at 5 K with a peak field up to ±1 T. For each field step, a constant magnetic field was applied and the remanence was measured after removal of the field and a delay of 120 s. The hysteresis loops were measured in fields of ±3 T at 5 and 300 K, respectively (Cao et al. 2010).

Relaxivity analysis The M-HFn-PEG nanoparticles were prepared using ddH_2O in 1.5 mL glass test tubes with iron concentrations from 0 to 0.2 mM. The measurement was carried out on a SPEC nuclear magnetic resonance with a field of 0.07 T (larmor frequency: 3 MHz) at room temperature. T_2 (transverse relaxation time) was measured using CPMG sequence. The echo time was 0.6 ms and the number of echoes collected was 8192. T_1 (longitudinal relaxation time) was measured using an inversion recovery sequence.

Thermal stability test Nine 1 mg/mL M-HFn-PEG nanoparticle samples were incubated in 0.1 M PBS buffer for 15 min at 60, 65, 70, 75, 80, 85, 90, 95, and 99 °C, respectively. The secondary structure of M-HFn-PEG shells was analyzed using CD spectra as described above.

Results

PEGylation of HFn

The SDS-PAGE method, which is sensitive to proteins with different molecular weight, was used to examine the PEGylation of HFn proteins. The PEG moiety was detected by barium iodide staining, based on the formation of a barium iodide complex with PEG (Kurfurst 1992). Figure 1a depicts the SDS-PAGE electrophoresis analysis of HFn PEGylation with different molecular weights in barium iodide staining. The lane 1 (HFn) is empty because the non-PEGylated HFn did not form a complex and was thus unable to be detected by barium iodide staining. Lane 2 and lane 3 clearly indicated the PEGylated HFn. The band in lane 3 (HFn-PEG20K) migrated slower than lane 2 (HFn-PEG10K). The barium iodide staining experiment confirms that HFn was linked with PEG molecules. Moreover, PEGylation with different molecular ratios, HFn subunit:PEG = 1:1, 1:2, 1:4, respectively, was also examined by the SDS-PAGE electrophoresis analysis. As seen in Fig. 1b, PEG was linked to HFn proteins.

Structure of M-HFn-PEG nanoparticles

Figure 2a shows the synthesized M-HFn-PEG nanoparticles have uniform core grain size. The nearly spherical shape of these nanoparticles indicates a good control in the mineralization of iron core by the PEGylated HFn protein shells. High-resolution TEM images (Fig. 2b) show lattice fringes of magnetite (Fe_3O_4). The size distribution and averaged core size of M-HFn_{5000}, M-HFn-$PEG10K_{5000}$, and M-HFn-$PEG20K_{5000}$ nanoparticles are shown in Fig. 2c. Specifically, the magnetite core sizes of M-HFn_{5000}, M-HFn-$PEG10K_{5000}$, and M-HFn-$PEG20K_{5000}$ nanoparticles are 4.8 ± 1.1, 5.2 ± 1.1, 5.6 ± 1.4 nm, respectively. A U-test indicates that the difference between means is very significant (p value is

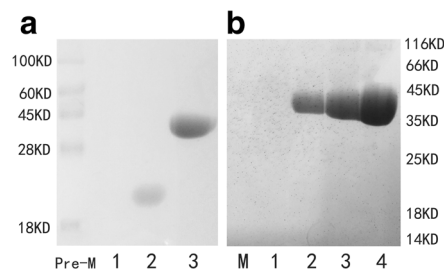

Fig. 1 **a** SDS-PAGE electrophoresis analysis of PEGylation with different molecular weights in barium iodide staining. Lane Pre-M, 1, 2, and 3, are protein preview marker, non-PEGylated HFn, HFn-PEG10K and HFn-PEG20K, respectively. **b** SDS-PAGE electrophoresis analysis of HFn PEGylation with different modification ratios in barium iodide staining. Lane M, 1, 2, 3, and 4, are protein marker, non-PEGylated HFn, HFn-PEG20K(1:1), HFn-PEG20K(1:2), HFn-PEG20K(1:4), respectively

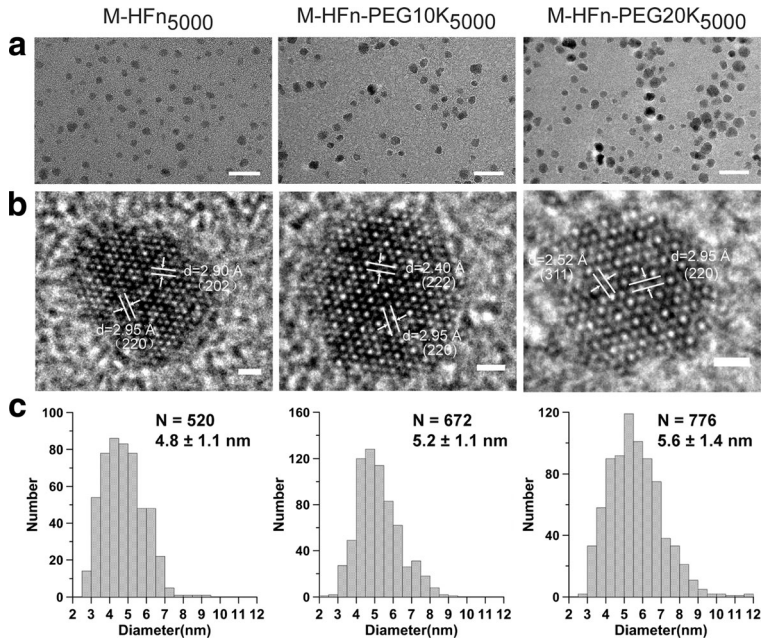

Fig. 2 Transmission electron microscopy (TEM) analysis of M-HFn nanoparticles and M-HFn-PEG nanoparticles (PEGylated with different molecular weights). **a** TEM micrographs of M-HFn_{5000}, M-HFn-$PEG10K_{5000}$, and M-HFn-$PEG20K_{5000}$ nanoparticles. *Scale bar* is 20 nm. **b** The high-resolution TEM images showing the lattice fringes of magnetite cores. *Scale bar* is 1 nm. **c** Histograms of size distributions and mean sizes of M-HFn_{5000}, M-HFn-$PEG10K_{5000}$, and M-HFn-$PEG20K_{5000}$ nanoparticles

less than 0.01). It is noted that the core size of M-HFn-$PEG10K_{5000}$ and M-HFn-$PEG20K_{5000}$ nanoparticles is slightly larger than that of M-HFn_{5000} nanoparticles.

Figure 3 shows the TEM analysis of M-HFn nanoparticles PEGylated with different molecular ratios. In Fig. 3a, the M-HFn-PEG nanoparticles with different modification ratios possess monodisperse, nearly spherical shaped magnetite cores. The core sizes of M-HFn_{5000}, M-HFn-$PEG20K(1:1)_{5000}$, M-HFn-$PEG20K(1:2)_{5000}$, and M-HFn-$PEG20K(1:4)_{5000}$ nanoparticles are 4.8 ± 1.1, 5.0 ± 1.0, 5.2 ± 1.0, 5.6 ± 1.3 nm, respectively (Fig. 3c). A U-test indicates that the difference between means is

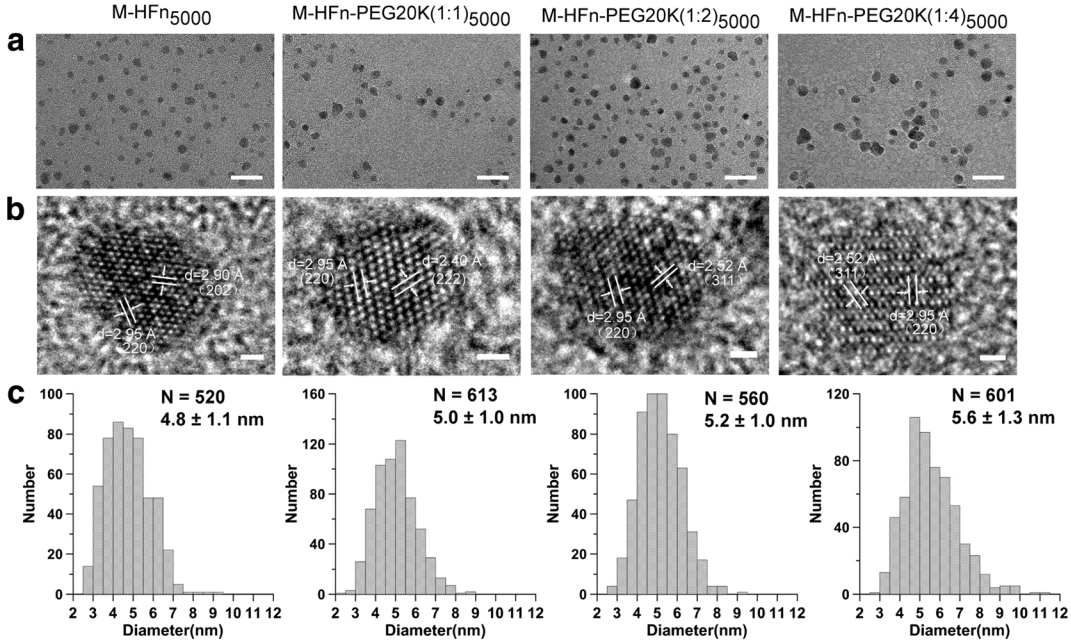

Fig. 3 TEM analysis of M-HFn nanoparticles PEGylated with different modification ratios. **a** TEM micrographs of M-HFn_{5000}, M-HFn-$PEG20K(1:1)_{5000}$, M-HFn-$PEG20K(1:2)_{5000}$, M-HFn-$PEG20K(1:4)_{5000}$ nanoparticles. **b** The high-resolution TEM images. *Scale bar* is 1 nm. **c** Size distributions of M-HFn nanoparticles with different PEG modification ratios

significant (p value is less than 0.05). Again, it indicates that the core size of M-HFn-PEG is slightly larger than that of M-HFn. When the molecular ratio is increased, the core size becomes slightly larger. Together, the results of our study suggest that the PEGylation of HFn may enhance magnetite core biomineralization.

Figure 4 shows that on CD spectra there is no evident difference between synthesized M-HFn and M-HFn-PEG nanoparticles from the pure HFn protein cages. The spectra similarity between M-HFn$_{5000}$, M-HFn-PEG10K$_{5000}$, M-HFn-PEG20K$_{5000}$ nanoparticles, and pure HFn protein indicates these nanoparticles possess a nearly intact protein cage after mineralization.

Magnetism of M-HFn-PEG nanoparticles

The saturation remanence (M_{rs}), saturation magnetization (M_s), coercivity (B_c), T_b and R value of synthesized M-HFn-PEG nanoparticles are present in Table 1. Notably, both at 5 K and 300 K, the M_{rs}, M_s, B_c, and T_b are increase with the PEG molecular weights or modification ratios.

As expected, at 300 K, there is no measurable coercivity and all M-HFn-PEG nanoparticles are superparamagnetic. At this temperature, the M_s of M-HFn$_{5000}$, M-HFn-PEG10K$_{5000}$, and M-HFn-PEG20K$_{5000}$ (the same batch) is 12.9, 15.3, and 22.2 Am^2/kg, respectively. While M_s of M-HFn-PEG20K(1:1)$_{5000}$, M-HFn-PEG20K(1:2)$_{5000}$, and M-HFn-PEG20K(1:4)$_{5000}$ is 14.7, 14.7, and 18 Am^2/kg, respectively. Note that the M-HFn-PEG20K(1:4)$_{5000}$ has unexpectedly high magnetic values compared with the corresponding M-HFn-PEG20K$_{5000}$., which is likely due to slight oxidation of the sample during a longer storage of former before magnetic measurement (Readman and O'reilly 1972). At 5 K, comparisons between T_b, M_{rs}/M_s (5 K), and B_c (5 K) values from the various samples are indicative of changes in the sizes of the magnetite cores, with larger cores corresponding to increased PEG molecular weight or ratio. This is consistent with the TEM observations (Figs. 2 and 3).

Based on the Wohlfarth-Cisowski test, for non-interacting single-domain particles, the IRM acquisition and DC demagnetization cross $R = 0.5$ (Cisowski 1981). Here, the R values of M-HFn-PEG nanoparticles are slightly less than 0.5 (Table 1), suggesting only weak magnetic interactions between our nanoparticles.

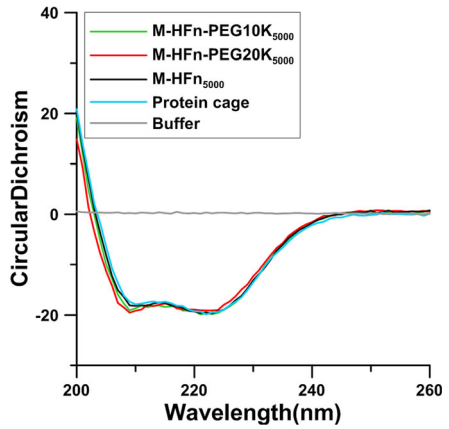

Fig. 4 The CD spectra showing secondary structures of pure HFn protein cages, M-HFn, and M-HFn-PEG nanoparticles

Iron content of M-HFn-PEG nanoparticles

The ICP-MS analysis indicates that the average iron content per protein of the synthesized M-HFn$_{5000}$, M-HFn-PEG10K$_{5000}$, and M-HFn-PEG20K$_{5000}$ nanoparticles was (2284), (3520), and (4940) Fe atoms, respectively. The average iron content of the synthesized M-HFn$_{5000}$, M-HFn-PEG20K(1:1)$_{5000}$, M-HFn-PEG20K(1:2)$_{5000}$, and M-HFn-PEG20K(1:4)$_{5000}$ nanoparticles was (2284), (2397), (2622), and (3277) Fe atoms per protein, respectively. It is evident that there are more iron atoms in the M-HFn-PEG nanoparticles than that of M-HFn nanoparticles. This is consistent with results of magnetic and TEM observations, which indicates larger magnetite cores.

Relaxivity analysis of M-HFn-PEG nanoparticles

Superparamagnetic iron oxide nanoparticles can accelerate the longitudinal relaxation of water protons and exhibit bright contrast. Meanwhile, superparamagnetic iron oxide nanoparticles also shorten the transverse relaxation time of water protons leading to a darkening of the MR images (Aime et al. 2005). Therefore, the magnetic nanoparticles can be used as MRI contrast agents (Bulte and Kraitchman 2004; Koenig and Kellar 1995). In the present study, we have measured the T_1 and T_2 of the synthesized M-HFn-PEG nanoparticles. Results of r_1 (longitudinal relaxivity, mM^{-1} s^{-1}) and r_2 (transverse relaxivity, mM^{-1} s^{-1}) are displayed in Fig. 5. As seen in Fig. 5, the relaxivity of M-HFn-PEG nanoparticles (i.e., using PEGylated HFn templates) is substantially increased compared to M-HFn nanoparticles (i.e., using non-PEGylated HFn templates).

Table 1 Magnetic parameters of synthesized PEGylated ferrimagnetic nanoparticles with different PEG molecular weights and different molecular ratios

Sample	M_{rs} (5 K) (Am^2/kg)	M_s (5 K) (Am^2/kg)	M_{rs}/M_s(5 K)	B_c (5 K) (mT)	M_s (300 K) (Am^2/kg)	T_b (K)	R
M-HFn$_{5000}$	3.8	16.9	0.22	11.6	12.9	17	0.47
M-HFn-PEG10K$_{5000}$	5.6	19.4	0.29	19.4	15.3	27.1	0.46
M-HFn-PEG20K$_{5000}$	8.1	27	0.3	23.5	22.2	85.6	0.44
M-HFn-PEG20K(1:1)$_{5000}$	5.1	19.2	0.27	17	14.7	25	0.47
M-HFn-PEG20K(1:2)$_{5000}$	5.3	19.2	0.28	17	14.7	21.3	0.46
M-HFn-PEG20K(1:4)$_{5000}$	6.5	22.7	0.29	19.8	18	55	0.45

M-HFn ferrimagnetic H-ferritin, *M-HFn-PEG* ferrimagnetic PEGylated H-ferritin M_s saturation magnetization, M_{rs} saturation remanence, B_c coercivity, T_b blocking temperature, R magnetostatic interaction parameter

Specifically, the r_1 of M-HFn$_{5000}$, M-HFn-PEG10K$_{5000}$, M-HFn-PEG20K$_{5000}$, M-HFn-PEG20K(1:1)$_{5000}$, M-HFn-PEG20K(1:2)$_{5000}$, and M-HFn-PEG20K(1:4)$_{5000}$ nanoparticles is 7.7, 19.4, 30, 15, 16.3, and 26.3 $mM^{-1}\ s^{-1}$, respectively. The corresponding r_2 is 13.9, 29.6, 59, 22.5, 25.8, and 44.6 $mM^{-1}\ s^{-1}$, respectively. We note here that the r_1 and r_2 values of M-HFn$_{5000}$ are smaller than previous r_1 and r_2 values reported in Cai et al. (2015), which is due to a lower magnetic field (0.07 T) being used in the present study.

Thermal stability of M-HFn-PEG nanoparticles

Figure 6 presents the CD spectra of M-HFn$_{5000}$, M-HFn-PEG10K$_{5000}$, and M-HFn-PEG20K$_{5000}$ nanoparticles after a thermal treatment for 15 min at temperatures of 60–99 °C. For the non-PEGylated M-HFn$_{5000}$ nanoparticles, the intensity clearly decreased after heating at 75 °C, it further decreased at 80 °C, and the secondary structure nearly disappeared by 85 °C (Fig. 6a). In contrast, the CD spectra of the PEGylated M-HFn-

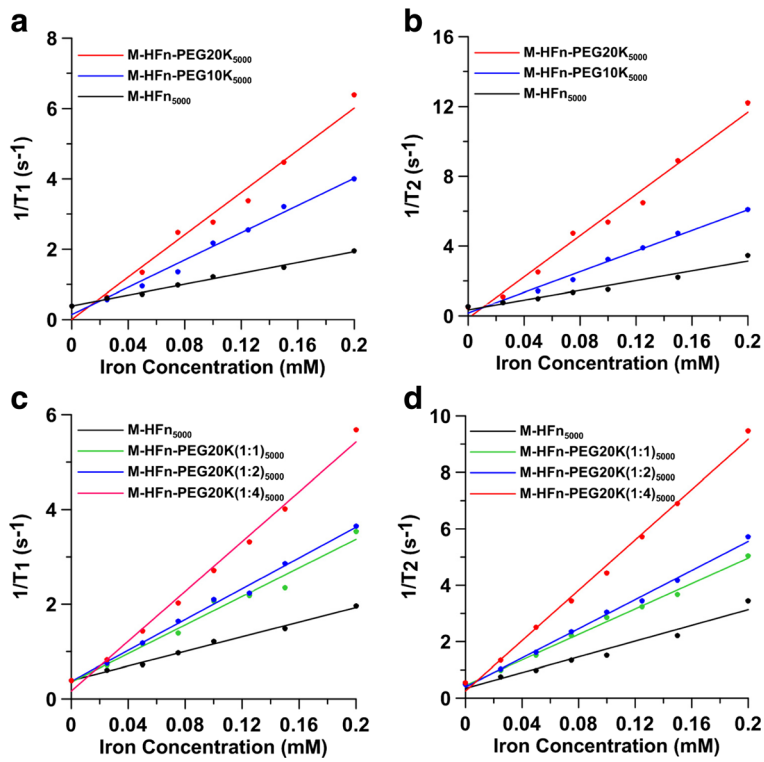

Fig. 5 Longitudinal relaxivity **(a, c)** and transverse relaxivity **(b, d)** analysis of M-HFn nanoparticles and M-HFn-PEG nanoparticles with different PEG molecular weights **(a, b)** and different modification ratios **(c, d)**

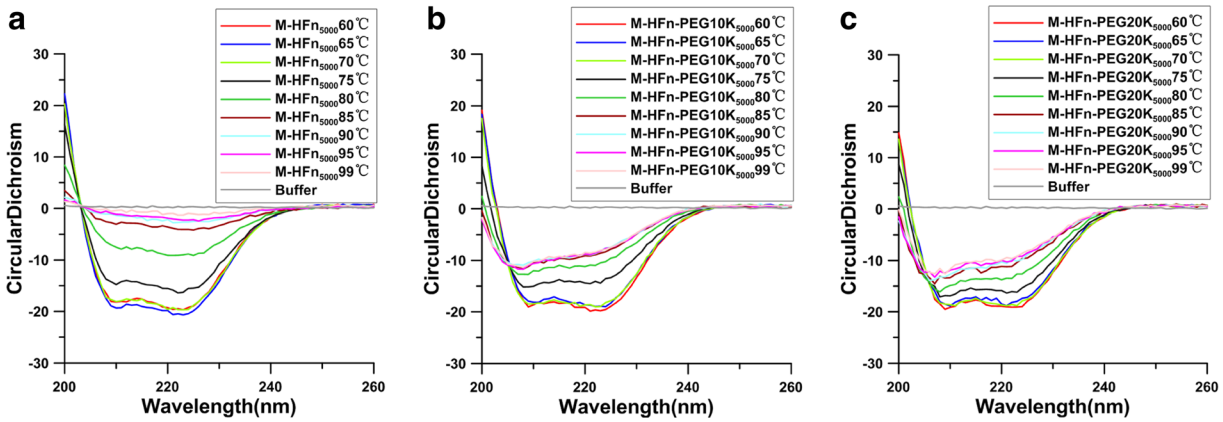

Fig. 6 The thermal stability of protein shells of M-HFn$_{5000}$ **(a)**, M-HFn-PEG10K$_{5000}$ **(b)**, and M-HFn-PEG20K$_{5000}$ **(c)** nanoparticles

PEG10K$_{5000}$ and M-HFn-PEG20K$_{5000}$ nanoparticles indicate much better thermal stability. The secondary structures nearly persisted up to 99 °C (Fig. 6b, c). This indicates that modification by PEG molecular weight (e.g., PEG20K) has improved the thermal stability of the protein cages. This observation is important because higher thermal stability can improve the application of ferritin (e.g., enzyme) in a wide variety of environmental and experimental conditions (Gaertner and Puigserver 1992; Rodriguez-Martinez et al. 2009; Treethammathurot et al. 2008; Zhang et al. 1999). Consequently, PEGylated M-HFn-PEG nanoparticles are of commercial importance for applications where biocatalysts are used under extreme conditions.

Iron uptake of HFn-PEG

Kinetic curves of ferrous oxidation analysis by non-PEGylated HFn and different PEGylated HFn-PEG nanoparticles are presented in Fig. 7. The absorbance of HFn-PEG10K and HFn-PEG20K is higher than that of HFn, and HFn-PEG20K is higher than HFn-PEG10K (Fig. 7a). In the Fig. 7b, the UV-Vis absorbance increases with increasing modification ratio. Together, these suggest that PEGylation modification of HFn may enhance the iron uptake of HFn. This rise of the iron uptake rate may be attributed to several factors including stabilization of the structure of the ferritin as well as maintaining a steady biomineralization microenvironment by PEGylation treatments (Tsukamoto et al. 2008).

Discussion

In the present study, the recombinant human H-chain ferritin (HFn) has been PEGylated by covalently linking PEG with different molecular weights (i.e., PEG10K and PEG20K), and with different molecular ratios (HFn subunit:PEG20K = 1:1, 1:2, 1:4), on its outer surface. PEG is an amphiphilic monodisperse polymer with a high degree of segmental flexibility in aqueous solutions. Our experiments show that monodispersed ferrimagnetic magnetoferritin M-HFn-PEG nanoparticles were

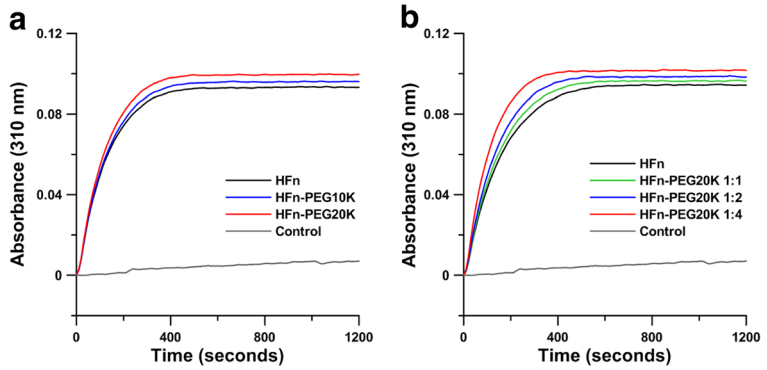

Fig. 7 The ferrous oxidation analysis of HFn and PEGylated HFn

successfully synthesized using these PEGylated HFn. From the circular dichroism spectra data, there is no significant difference between the pure HFn, non-PEGylated M-HFn protein shell, and the PEGylated M-HFn-PEG protein shell. It suggests that the PEGylation does not significantly change the structure and function of HFn. A good monodispersity of the M-HFn-PEG nanoparticles (Figs. 2 and 3) also supports an intact protein cage of the M-HFn-PEG magnetoferritin.

The commonly supposed structure of PEGylated protein is the shell-like model that a conjugated PEG chain surrounded the protein to form a PEG layer (Fee and Van Alstine 2004; Garcia-Arellano et al. 2002). Collectively, the PEG chain formed a PEG layer around ferritin, which provides good protection for the ferritin. When temperature rises, the hydrophilic PEG chains wrap around ferritin and forms a highly hydrogen-bonded structure (Gaertner and Puigserver 1992; Zhang et al. 1999), giving the PEGylated ferritin the capability to withstand higher temperatures. This is confirmed by our thermal stability test data (Fig. 6). Moreover, research has shown that the PEG wraps also prevent aggregation (Castellanos et al. 2003). In this regard, the possible role played by PEG could be explained as follows. On one hand, the PEG shell was expected to stabilize the structure of the ferritin. On the other hand, the attached PEG acted to create a dynamic, hydrated polymer-rich layer at the ferritin surface that maintained a steady microenviroment and inhibited precipitation on it. Further experiments are still needed to investigate the true function of PEGylation on thermal stability and uptake of iron.

Here the ferrous oxidation and iron content data measured by ICP-MS of HFn and PEGylated HFn reveals a higher iron uptake activity of PEGylated ferritin, which indicates that PEGylation may promote the synthesis of the magnetite nanoparticles using the HFn-PEG protein cavity as a nanoplatform. The TEM observations and magnetic measurements confirm that PEGylation slightly increases the overall magnetite core size and mineralization of magnetite M-HFn-PEG nanoparticles. The average diameter, blocking temperature, saturation magnetization, and relaxivity of different M-HFn-PEG nanoparticles are higher compared with non-PEGylated M-HFn nanoparticles. Our new results show that PEG modification of HFn may enhance the biomineralization of HFn proteins. Nevertheless, the mechanism remains unknown and further investigation is required.

Conclusions

The following conclusions can be drawn from this study.

1. PEGylation of the outer surface of the recombinant human HFn has been successfully modified with different PEG molecular weighs and PEG modification ratios.
2. Biomimetic synthesis of magnetite cores has been carried out using these PEGylated HFn nanoparticles. We found that the protein cages of the formed M-HFn-PEG nanoparticles were nearly intact. TEM observation indicates that the synthesized magnetite cores of M-HFn-PEG nanoparticles are monodispersed, well crystalline and nearly spherical in shape.
3. With increased PEG molecular weight or modification ratio, the M-HFn-PEG nanoparticles have slightly larger core size, magnetization, coercivity, iron content, relaxivity, iron uptake rate, and thermal stability. Together, these suggest that PEGylation of HFn could improve the magnetite core synthesis of magnetoferritin nanoparticles.
4. Possible roles played by PEGylation on HFn may include stabilizing the structure of ferritin and providing a steady microenviroment for iron uptake and biomineralization.

Acknowledgments We thank colleagues Naigui Liu at NMR sub-laboratory for help in the relaxivity experiment, Xu Tang and Lixin Gu at Transmission Electron Microscopy Laboratory for their help in TEM experiments, and Greig A. Paterson for language editing. This work was supported by grants of the National Natural Science Foundation of China (41621004, 41330104, and 41574062) and the Frontier Science Program of Chinese Academy of Sciences.

Compliance with ethical standards

Conflict of interest The authors declare that they have no conflict of interest.

References

Aime S, Botta M, Terreno E (2005) Gd(III)-based contrast agents for MRI. Adv Inorg Chem 57:173–237. doi:10.1016/S0898-8838(05)57004-1

Bulte JWM, Kraitchman DL (2004) Iron oxide MR contrast agents for molecular and cellular imaging. NMR Biomed 17:484–499. doi:10.1002/nbm.924

Burda C, Chen XB, Narayanan R, El-Sayed MA (2005) Chemistry and properties of nanocrystals of different shapes. Chem Rev 105:1025–1102. doi:10.1021/cr030063a

Burtea C, Laurent S, Roch A, Elst LV, Muller RN (2005) C-MALISA (cellular magnetic-linked immunosorbent assay), a new application of cellular ELISA for MRI. J Inorg Biochem 99(5):1135–1144. doi:10.1016/j.jinorgbio.2005.02.009

Cai Y, Cao CQ, He XQ, Yang CY, Tian LX, Zhu RX, Pan YX (2015) Enhanced magnetic resonance imaging and staining of cancer cells using ferrimagnetic H-ferritin nanoparticles with increasing core size. Int J Nanomedicine 10:2619–2634. doi:10.2147/Ijn.S80025

Cao CQ, Tian LX, Liu QS, Liu WF, Chen GJ, Pan YX (2010) Magnetic characterization of noninteracting, randomly oriented, nanometer-scale ferrimagnetic particles. J Geophys Res-Sol Ea 115. doi:10.1029/2009jb006855

Cao CQ, Wang XX, Cai Y, Sun L, Tian LX, Wu H, He XQ, Lei H, Liu WF, Chen GJ, Zhu RX, Pan YX (2014) Targeted in vivo imaging of microscopic tumors with ferritin-based nanoprobes across biological barriers. Adv Mater 26:2566–2571. doi:10.1002/adma.201304544

Castellanos IJ, Crespo R, Griebenow K (2003) Poly(ethylene glycol) as stabilizer and emulsifying agent: a novel stabilization approach preventing aggregation and inactivation of proteins upon encapsulation in bioerodible polyester microspheres. J Control Release 88:135–145. doi:10.1016/S0168-3659(02)00488-1

Cisowski S (1981) Interacting vs non-interacting single domain behavior in natural and synthetic samples. Phys Earth Planet Inter 26:56–62. doi:10.1016/0031-9201(81)90097-2

Delgado C, Francis GE, Fisher D (1992) The uses and properties of PEG-linked proteins. Crit Rev Ther Drug Carrier Syst 9: 249–304

Ding HL, Zhang YX, Wang S, Xu JM, Xu SC, Li GH (2012) Fe_3O_4@SiO_2 core/shell nanoparticles: the silica coating regulations with a single core for different core sizes and shell thicknesses. Chem Mater 24:4572–4580. doi: 10.1021/cm302828d

Douglas T, Dickson DPE, Betteridge S, Charnock J, Garner CD, Mann S (1995) Synthesis and structure of an iron(iii) sulfide-ferritin bioinorganic nanocomposite. Science 269:54–57. doi:10.1126/science.269.5220.54

Dreaden EC, Alkilany AM, Huang XH, Murphy CJ, El-Sayed MA (2012) The golden age: gold nanoparticles for biomedicine. Chem Soc Rev 41:2740–2779. doi:10.1039/c1cs15237h

Falvo E, Tremante E, Fraioli R et al (2013) Antibody-drug conjugates: targeting melanoma with cisplatin encapsulated in protein-cage nanoparticles based on human ferritin. Nanoscale 5:12278–12285. doi:10.1039/c3nr04268e

Fan J, Lu J, Xu R, Jiang R, Gao Y (2003) Use of water-dispersible Fe_2O_3 nanoparticles with narrow size distributions in isolating avidin. J Colloid Interface Sci 266(1):215–218. doi:10.1016/S0021-9797(03)00570-8

Fan K, Cao C, Pan Y et al (2012) Magnetoferritin nanoparticles for targeting and visualizing tumour tissues. Nat Nanotechnol 7: 459–464. doi:10.1038/nnano.2012.90

Fantechi E, Innocenti C, Zanardelli M et al (2014) A smart platform for hyperthermia application in cancer treatment: cobalt-doped ferrite nanoparticles mineralized in human ferritin cages. ACS Nano 8:4705–4719. doi:10.1021/nn500454n

Fee CJ, Van Alstine JM (2004) Prediction of the viscosity radius and the size exclusion chromatography behavior of PEGylated proteins. Bioconjug Chem 15:1304–1313. doi:10.1021/bc049843w

Gaertner HF, Puigserver AJ (1992) Increased activity and stability of poly(ethylene glycol)-modified trypsin enzyme. Microb Tech 14:150–155. doi:10.1016/0141-0229(92)90174-M

Gao JH, Gu HW, Xu B (2009) Multifunctional magnetic nanoparticles: design, synthesis, and biomedical applications. Accounts Chem Res 42:1097–1107. doi:10.1021/ar9000026

Garcia-Arellano H, Valderrama B, Saab-Rincon G, Vazquez-Duhalt R (2002) High temperature biocatalysis by chemically modified cytochrome c. Bioconjug Chem 13:1336–1344. doi:10.1021/bc025561p

Harris JM, Chess RB (2003) Effect of pegylation on pharmaceuticals. Nat Rev Drug Discov 2:214–221. doi:10.1038/nrd1033

Harrison PM, Arosio P (1996) The ferritins: molecular properties, iron storage function and cellular regulation. Biochim Biophys Acta 1275:161–203. doi:10.1016/0005-2728(96)00022-9

Harrison PM, Fischbac FA, Hoy TG, Haggis GH (1967) Ferric oxyhydroxide core of ferritin. Nature 216:1188–1190. doi: 10.1038/2161188a0

Hinds KD, Kim SW (2002) Effects of PEG conjugation on insulin properties. Adv Drug Deliver Rev 54:505–530. doi:10.1016/S0169-409x(02)00025-X

Kinstler OB, Brems DN, Lauren SL, Paige AG, Hamburger JB, Treuheit MJ (1996) Characterization and stability of N-terminally PEGylated rhG-CSF. Pharmaceut Res 13:996–1002. doi:10.1023/A:1016042220817

Koenig SH, Kellar KE (1995) Theory of $1/T_1$ and $1/T_2$ NMRD profiles of solutions of magnetic nanoparticles. Magn Reson Med 34:227–233. doi:10.1002/mrm.1910340214

Kohler N, Sun C, Fichtenholtz A (2006) Methotrexate-immobilized poly (ethylene glycol) magnetic nanoparticles for MR imaging and drug delivery. Small 2(6):785–792. doi:10.1002/smll.200600009

Kramer RM, Li C, Carter DC, Stone MO, Naik RR (2004) Engineered protein cages for nanomaterial synthesis. J Am Chem Soc 126:13282–13286. doi:10.1021/ja046735b

Kurfurst MM (1992) Detection and molecular-weight determination of polyethylene glycol-modified hirudin by staining after sodium dodecyl-sulfate polyacrylamide-gel electrophoresis. Anal Biochem 200:244–248. doi:10.1016/0003-2697(92)90460-O

Laurent S, Forge D, Port M, Roch A, Robic C, Elst LV, Muller RN (2010) Magnetic iron oxide nanoparticles: synthesis, stabilization, vectorization, physicochemical characterizations, and biological applications. Chem Rev 110:2574–2574. doi:10.1021/cr900197g

Lu YL, Harding SE, Turner A et al (2008) Effect of PEGylation on the solution conformation of antibody fragments. J Pharm Sci-US 97:2062–2079. doi:10.1002/jps.21170

Mann S, Meldrum FC (1991) Controlled synthesis of inorganic materials using supramolecular assemblies. Adv Mater 3: 316–318. doi:10.1002/adma.19910030611

Mann S, Archibald DD, Didymus JM, Douglas T, Heywood BR, Meldrum FC, Reeves NJ (1993) Crystallization at inorganic-organic interfaces-biominerals and biomimetic synthesis. Science 261:1286–1292. doi:10.1126/science.261.5126.1286

Matsumura S, Aoki I, Saga T, Shiba K (2011) A tumor-environment-responsive nanocarrier that evolves its surface

properties upon sensing matrix metalloproteinase-2 and initiates agglomeration to enhance T_2 relaxivity for magnetic resonance imaging. Mol Pharmaceut 8:1970–1974. doi:10.1021/mp2001999

Meldrum FC, Heywood BR, Mann S (1992) Magnetoferritin: in vitro synthesis of a novel magnetic protein. Science 257:522–523. doi:10.1126/science.1636086

Melnikova L, Pospiskova K, Mitroova Z, Kopcansky P, Safarik I (2014) Peroxidase-like activity of magnetoferritin. Microchim Acta 181:295–301. doi:10.1007/s00604-013-1105-5

Pankhurst Q, Jones S, Dobson J (2016) Applications of magnetic nanoparticles in biomedicine: the story so far. J Phys D Appl Phys 49(50):501002–501003. doi:10.1088/0022-3727/49/50/501002

Readman PW, O'reilly W (1972) Magnetic properties of oxidized (cation-deficient) titanomagnetites (Fe, Ti, □)$_3O_4$. J Geomag Geoelectr 24(1):69–90. doi: 10.5636/jgg.24.69

Roberts MJ, Bentley MD, Harris JM (2002) Chemistry for peptide and protein PEGylation. Adv Drug Deliv Rev 54:459–476. doi:10.1016/j.addr.2012.09.025

Rodriguez-Martinez JA, Rivera-Rivera I, Sola RJ, Griebenow K (2009) Enzymatic activity and thermal stability of PEG-alpha-chymotrypsin conjugates. Biotechnol Lett 31:883–887. doi:10.1007/s10529-009-9947-y

Theil EC (1987) Ferritin-structure, gene-regulation, and cellular function in animals, plants, and microorganisms. Annu Rev Biochem 56:289–315. doi:10.1146/annurev.biochem.56.1.289

Treethammathurot B, Ovartlarnporn C, Wungsintaweekul J, Duncan R, Wiwattanapatapee R (2008) Effect of PEG molecular weight and linking chemistry on the biological activity and thermal stability of PEGylated trypsin. Int J Pharmaceut 357:252–259. doi:10.1016/j.ijpharm.2008.01.016

Tromsdorf UI, Bruns OT, Salmen SC, Beisiegel U, Weller H (2009) A highly effective, nontoxic T-1 MR contrast agent based on ultrasmall PEGylated iron oxide nanoparticles. Nano Lett 9:4434–4440. doi:10.1021/nl902715v

Tsukamoto R, Muraoka M, Fukushige Y, Nakagawa H, Kawaguchi T, Nakatsuji Y, Yamashita I (2008) Improvement of Co_3O_4 nanoparticle synthesis in apoferritin cavity by outer surface pegylation. B Chem Soc Jpn 81:1669–1674. doi:10.1246/bcsj.81.1669

Uchida M, Flenniken ML, Allen M et al (2006) Targeting of cancer cells with ferrimagnetic ferritin cage nanoparticles. J Am Chem Soc 128:16626–16633. doi:10.1021/ja0655690

Uchida M, Terashima M, Cunningham CH et al (2008) A human ferritin iron oxide nano-composite magnetic resonance contrast agent. Magn Reson Med 60:1073–1081. doi:10.1002/mrm.21761

Uchio T, Baudys M, Liu F, Song SC, Kim SW (1999) Site-specific insulin conjugates with enhanced stability and extended action profile. Adv Drug Deliver Rev 35:289–306. doi:10.1016/S0169-409x(98)00078-7

Vannucci L, Falvo E, Fornara M et al (2012) Selective targeting of melanoma by PEG-masked protein-based multifunctional nanoparticles. Int J Nanomedicine 7:1489–1509. doi:10.2147/Ijn.S28242

Veronese FM (2001) Peptide and protein PEGylation: a review of problems and solutions. Biomaterials 22:405–417. doi:10.1016/S0142-9612(00)00193-9

Walls MG, Cao CQ, Kui YZ, Li JH, Che RC, Pan YX (2013) Identification of ferrous-ferric Fe_3O_4 nanoparticles in recombinant human ferritin cages. Microsc Microanal 19:835–841. doi:10.1017/S1431927613001724

Wynn TT, Gumuscu B (2016) Potential role of a new PEGylated recombinant factor VIII for hemophilia a. Journal of blood medicine 7:121–128. doi:10.2147/JBM.S82457

Yamashita I, Hayashi J, Hara M (2004) Bio-template synthesis of uniform CdSe nanoparticles using cage-shaped protein, apoferritin. Chem Lett 33:1158–1159. doi:10.1246/Cl.2004.1158

Yu XG, Marks TJ, Facchetti A (2016) Metal oxides for optoelectronic applications. Nat Mater 15:383–396. doi:10.1038/NMAT4599

Zhang ZD, He ZM, Guan GQ (1999) Thermal stability and thermodynamic analysis of native and methoxypolyethylene glycol modified trypsin. Biotechnol Tech 13:781–786. doi:10.1023/A:1008900804320

Zhang T, Cao C, Tang X, Cai Y, Yang C, Pan Y (2017) Enhanced peroxidase activity and tumour tissue visualization by cobalt-doped magnetoferritin nanoparticles. Nanotechnology 28:045704. doi:10.1088/1361-6528/28/4/045704